Aerobic Granules: Microbial Landscape and Architecture, Stages, and Practical Implications

Graciela Gonzalez-Gil, Christof Holliger

École Polytechnique Fédérale de Lausanne, School of Architecture, Civil and Environmental Engineering, Laboratory for Environmental Biotechnology, Lausanne, Switzerland

For the successful application of aerobic granules in wastewater treatment, granules containing an appropriate microbial assembly able to remove contaminants should be retained and propagated within the reactor. To manipulate and/or optimize this process, a good understanding of the formation and dynamic architecture of the granules is desirable. Models of granules often assume a spherical shape with an outer layer and an inner core, but limited information is available regarding the extent of deviations from such assumptions. We report on new imaging approaches to gain detailed insights into the structural characteristics of aerobic granules. Our approach stained all components of the granule to obtain a high quality contrast in the images; hence limitations due to thresholding in the image analysis were overcome. A three-dimensional reconstruction of the granular structure was obtained that revealed the mesoscopic impression of the cavernlike interior of the structure, showing channels and dead-end paths in detail. In "old" granules, large cavities allowed for the irrigation and growth of dense microbial colonies along the path of the channels. Hence, in some areas, paradoxically higher biomass content was observed in the inner part of the granule compared to the outer part. Microbial clusters "rooting" from the interior of the mature granule structure indicate that granules mainly grow via biomass outgrowth and not by aggregation of small particles. We identify and discuss phenomena contributing to the life cycle of aerobic granules. With our approach, volumetric tetrahedral grids are generated that may be used to validate complex models of granule formation.

Granules are compact, quasispherical aggregates formed by self-immobilized, mixed microbial communities embedded in a matrix of extracellular bio-polymeric substances (1). The phenomenon of granule formation in wastewater treatment systems was first described in anaerobic bioreactors (2, 3). The technological success of anaerobic granules in the treatment of highly concentrated industrial wastewaters (4) has been crucial to stimulating research in developing their aerobic counterparts. Previous studies have shown that in sequencing batch reactors and under certain operational conditions, which include high shear stress and short settling times (5), activated sludge can form aerobic granules (5, 6). Compared to flocs, granules can accommodate five times the biomass concentration (7) and settle 10 times faster (8, 9), and these characteristics translate into small-footprint wastewater treatment plants. Therefore, the use of aerobic granular sludge-based systems stands as a promising alternative technology to conventional activated sludge treatment systems (10). To guarantee the successful application of the aerobic granular sludge technology, granules should be physically stable and should contain an appropriate microbial assembly able to remove the desired contaminants. Moreover, in the long term, this assembly should be retained and should propagate within the reactor and should be resistant to environmental changes. Most research thus far has focused on the engineering aspects of the reactors and on operational variables necessary to induce granulation (11–16). Recently, at a molecular level, the makeup of the microbial assemblies of the aggregates has been studied for aerobic granules under different conditions (17–19). Aerobic granules exposed to temporal anaerobic-aerobic cycles display the ability to biologically remove phosphorus and nitrogen in a single reactor (7). Mathematical simulations show that bulk oxygen concentrations of 2 mg liter^{-1} and granules sizes between 1.2 to 1.4 mm would be required for optimum nutrient removal because such conditions

would result in an appropriate ratio of aerobic to anoxic volumes within the granule (20). Conceptual and mathematical models of granules assume a spherical shape with an outer layer and an inner core. Although this approach has increased our understanding of the process, models are often only validated against macroscale results with limited or no microscale observations (21, 22). Despite the fact that the physical architecture of the granules is intrinsically related to mass transport, conversion processes and niches partitioning within the granules, few reports describe details on the microstructure of aerobic granules (23, 24). In addition, an effective approach to stain all of the constituents of the aggregates is required because most previous research has focused on fluorescence methods to target specific bacterial types. To better understand granule architecture and function, we (i) explored a different approach to the staining and imaging of the granular structure and (ii) reconstructed the granular sludge in three dimensions.

MATERIALS AND METHODS

Origin of granule samples. Aerobic granules with highly enhanced biological phosphorus removal capacity were obtained from two 2.4-liter sequencing batch reactors fed with propionate or acetate, as described
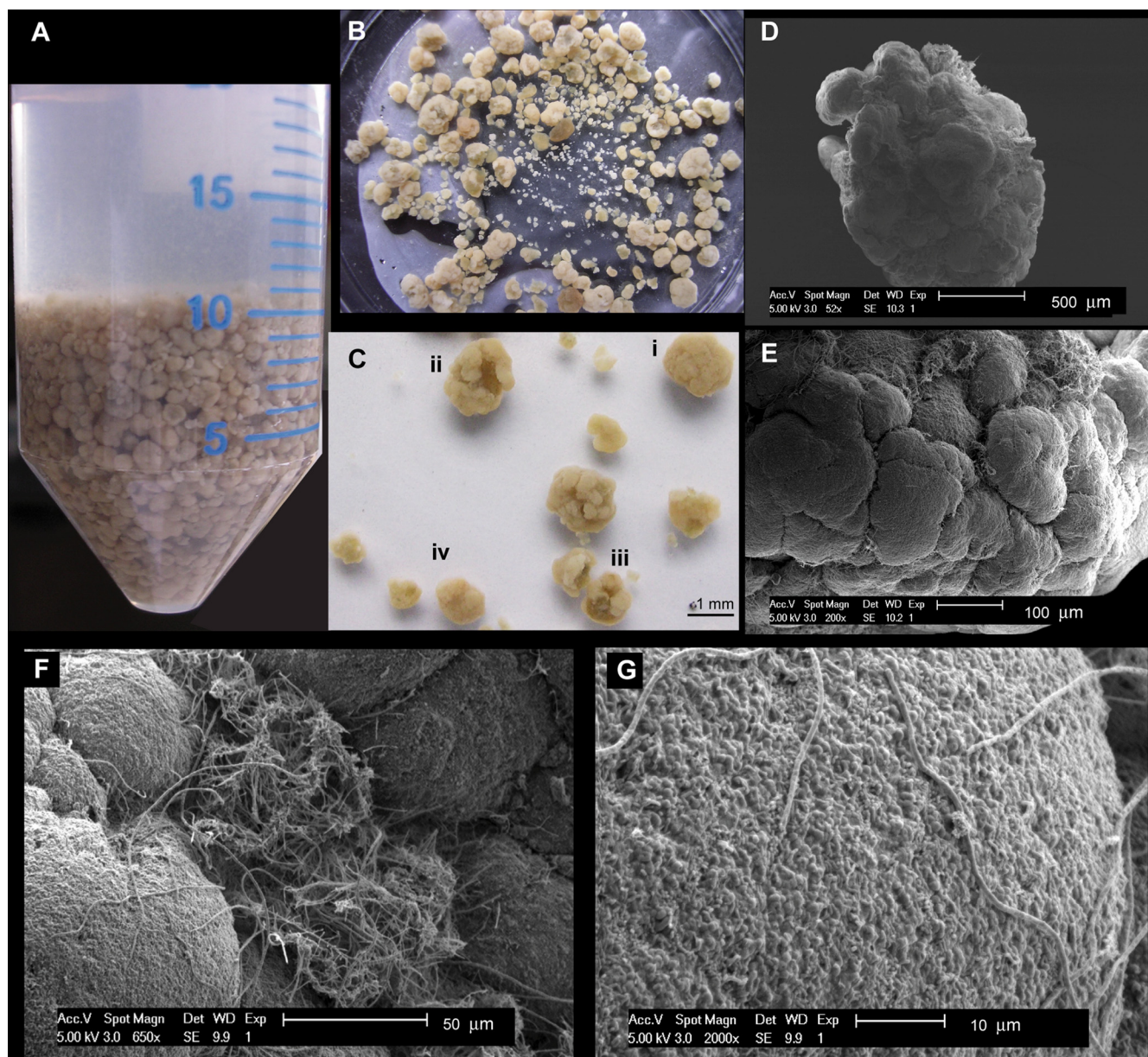
FIG 1 (A) Macroimpression of aerobic granular sludge. (B) Granules grown in propionate and sampled at day 169. (C) Stereomicrograph of granules having different "life" stage (see the text). (D) Low-magnification SEM image of a granule showing large clusters. (E) SEM image of the surface of a granule. (F) Zoom image of panel E reveals some filamentous bacteria sheltered between clusters. (G) Detailed impression of the surface of a cluster.

previously in detail (18). Briefly, the reactors were inoculated with activated sludge from the Uetendorf sewage treatment plant, Thun, Switzerland; a plant that removes N and P biologically. The reactors were operated at 20°C in a sequencing batch mode with 3-h cycles consisting of an anaerobic feeding phase at a flow rate of 1.2 liters h^{-1} (60 min), an aeration phase with airflow rate at 4 liters min^{-1} (112 min), a settling phase (3 min), and a withdrawal phase (5 min). The pH was controlled at 7 to 7.3. The composition of the synthetic wastewater used to feed the reactors was as given previously (7). The organic loading rate for both reactors was 1.8 g of chemical oxygen demand (COD) $liter^{-1}$ day^{-1}. The oxygen concentration was maintained at saturation levels during the aerobic phase.

Preparation of thin sections of granules. Granules were fixed overnight at 4°C in 4% formaldehyde in phosphate-buffered saline (PBS; pH 7.4). The granules were then washed three times with PBS and stored overnight at 20°C in a PBS-ethanol solution (1:1 [vol/vol]). The granules were then dehydrated using an ethanol series of 50, 80, and 100%, with 20 min per step. Dehydrated samples were cleared with xylene to remove any remaining ethanol and then infiltrated with and embedded in paraffin wax. Granule sections 12 μm thick were obtained with a microtome (Microm, catalog no. HM360) and placed on Superfrost^Plus slides (Menzel-Gläzer, Braunschweig, Germany).

FISH. After the paraffin was removed using xylene (two treatments for 20 min each time), followed by washing in 100% ethanol for 5 min, a section corresponding to the center of the granule was subjected to fluorescence *in situ* hybridization (FISH) procedures, as reported earlier (25), with a mixture of the following probes: Cy3-labeled PAO (PAO462, PAO651, and PAO846) (26) and FAM-labeled GAO (GAOQ431, GAOQ989, and GB_G2) (27, 28). The final concentrations of each Cy3-
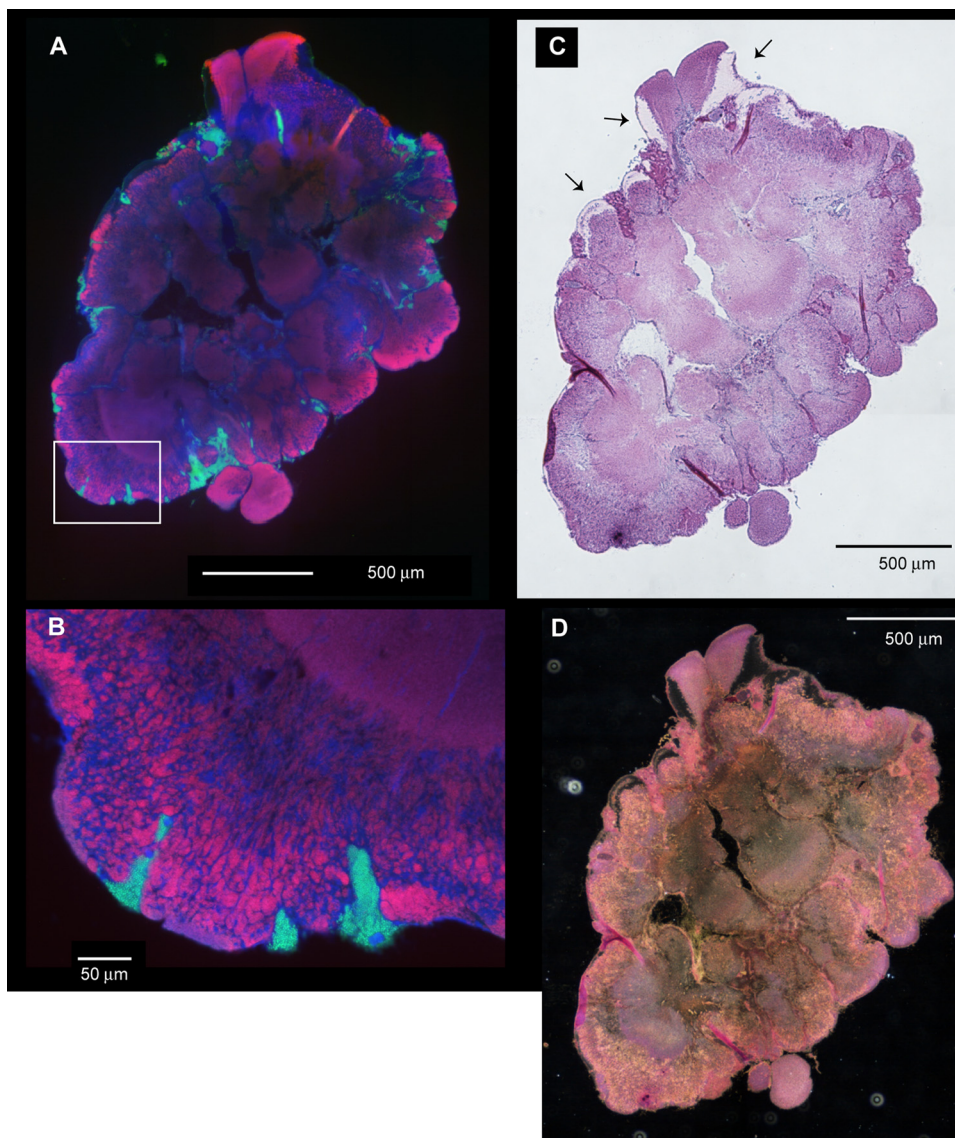
FIG 2 Thin section images of a propionate-cultivated granule sampled at day 169. (A) Fluorescence image showing large clusters of *Accumulibacter*-like bacteria in pink. *Competibacter*-like bacteria are shown in cyan and other microorganisms are shown in blue. (B) Zoom image corresponding to the box in panel A showing growing clusters. (C and D) Bright-field and dark-field images, respectively, of a contiguous section to that in panel A and stained with H&E. The arrows in panel C indicate glue-like structures.

labeled and FAM-labeled probe were 3 and 5 ng ml^{-1}, respectively, and the hybridization conditions were as previously described (26–28). After the unbound probes were removed, the sections were counterstained with 20 μg of DAPI (4′,6′-diamidino-2-phenylindole)/ml for 20 min under dark conditions, washed with cold distilled water, and air-died before being mounted with AF1 antifade solution (Citifluor, London, England). The hybridized sections were observed and documented using a Leica DM5500 fluorescence microscope and its associated software.

H&E staining. For hematoxylin-eosin (H&E) treatment, the sections were deparaffinized in xylene and hydrated. The sections were stained with hematoxylin for 10 min, washed with water for 10 min, and counterstained with eosin for 2 min. The sections were then dehydrated using an ethanol series (70, 96, and 100%, three times for 2 min each time), cleared with xylene (twice for 2 min each time), and mounted in Cytoseal 60 (Micron International). The thin sections were observed using a Leica DM5500 microscope in bright-field mode and documented using a DFC 320 R2 camera with the Leica Application Suite software. Dark-field ob-

servations were conducted using a Nikon Eclipse E800 microscope and NIS elements software.

Scanning electron microscopy (SEM). Intact granules were prepared as described previously (29), and images were acquired using a Philips FEI XLF30 microscope at 5 kV.

Granule 3D reconstruction. Bright-field images of consecutive thin sections were used and registered (i.e., aligned) manually using Adobe Photoshop CS3. Thereafter, images were segmented to remove the background-related signal from the granule-related signal using the ImageJ software program (30) with the Color Segmentation plug-in, which is based on the k-mean algorithm (http://bigwww.epfl.ch/sage /soft/colorsegmentation/). From the results of the color segmentation, a binary mask was obtained using the threshold function in ImageJ (intensity = 1 and 0 for the granule and background-related signals, respectively). This binary mask was then multiplied by each channel of the RGB image (color segmented), and then the channels were merged. The images were then stacked and visualized in three dimensions (3D)
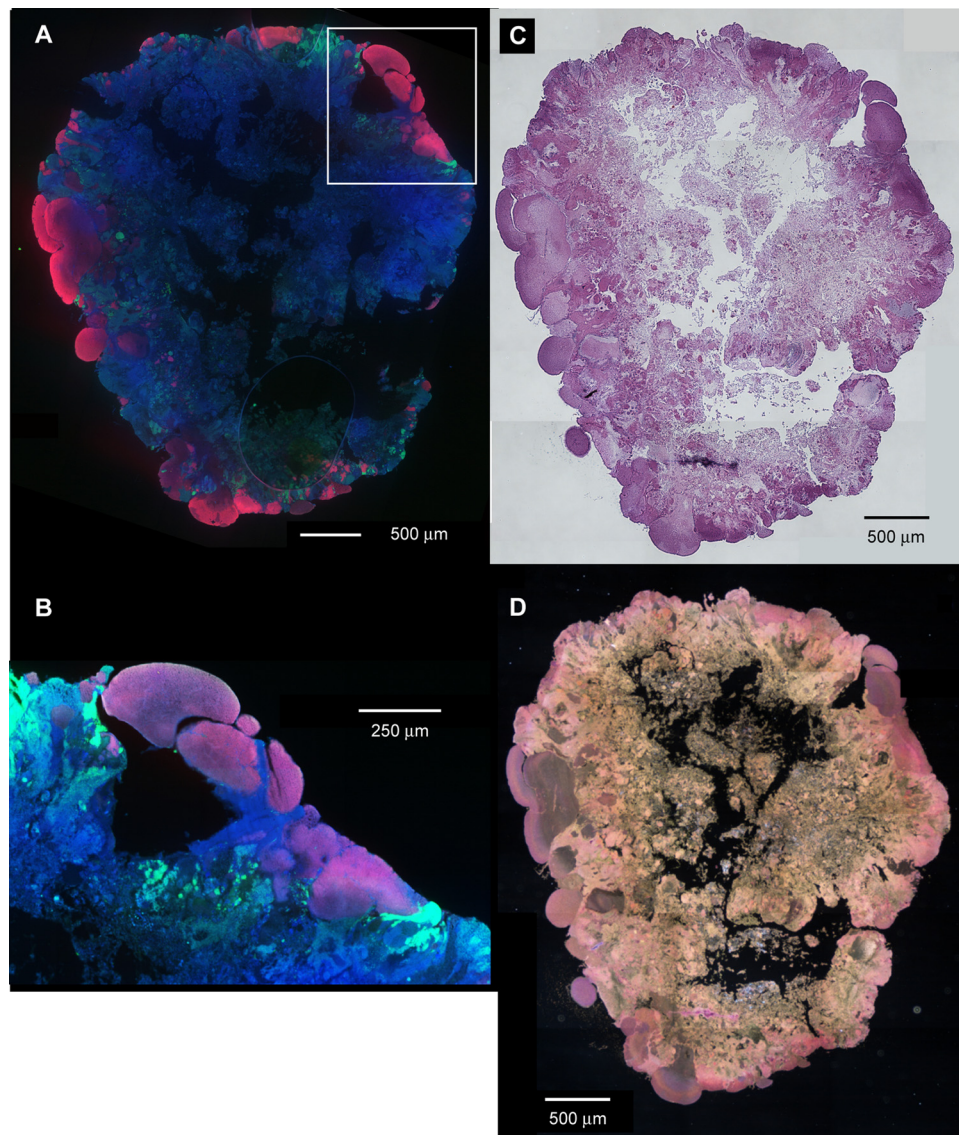
FIG 3 Thin section images of an acetate-cultivated granule sampled at day 169. (A) Fluorescence image showing clusters of *Accumulibacter*-like bacteria in pink. *Competibacter*-like bacteria are shown in cyan and other microorganisms are shown in blue. (B) Zoom image corresponding to the box in panel A. (C and D) Bright-field and dark-field images, respectively, of a contiguous section to that in panel A and stained with H&E showing the outgrow structure of the clusters.

using Avizo (Visualization Sciences Group) image-processing software. The image processing and handling was performed with a 64-bit, 32-GB RAM work station.

Estimation of granule characteristics from images. The fractal dimension of the granule was estimated by the box counting method as implemented in the ImageJ plug-in BoneJ (31). This method counts the number of boxes required to cover the ribbon of the object at a given box scale. The scale is subsequently changed and the box counting is repeated. The fractal dimension is computed as the ratio of the change in the log of the box count to the change in the log of the box scale (39). The fractal values obtained by this method vary between 1 and 2, with higher values indicating a more irregular shape. Using ImageJ, the porosity was estimated for each binary image corresponding to a different radial location and calculated as the percentage of voids with respect to the total area of the granule. Further details can be found in the supplemental material.

RESULTS

Cluster structure of aerobic granules. The general appearance of mature aerobic granules is shown in Fig. 1A and B. The population of mature granules was comprised of (i) quasispherical entities showing large cluster structures, (ii) quasispherical entities from which various clusters had been detached, (iii) quasi-half-broken granules, and (iv) small- and medium-sized newly growing granules from the detached clusters (Fig. 1C). These forms illustrate the life cycle of these mature granules (see Fig. S1 in the supplemental material). Low- and high-magnification SEM images show the cluster architecture of the granules in detail (Fig. 1D and E). The clusters are comprised of dense bacterial populations with coccus- and rod-like morphologies. Few bacterial filaments were found between cluster areas in which lower shear forces may exist (Fig. 1F and G).
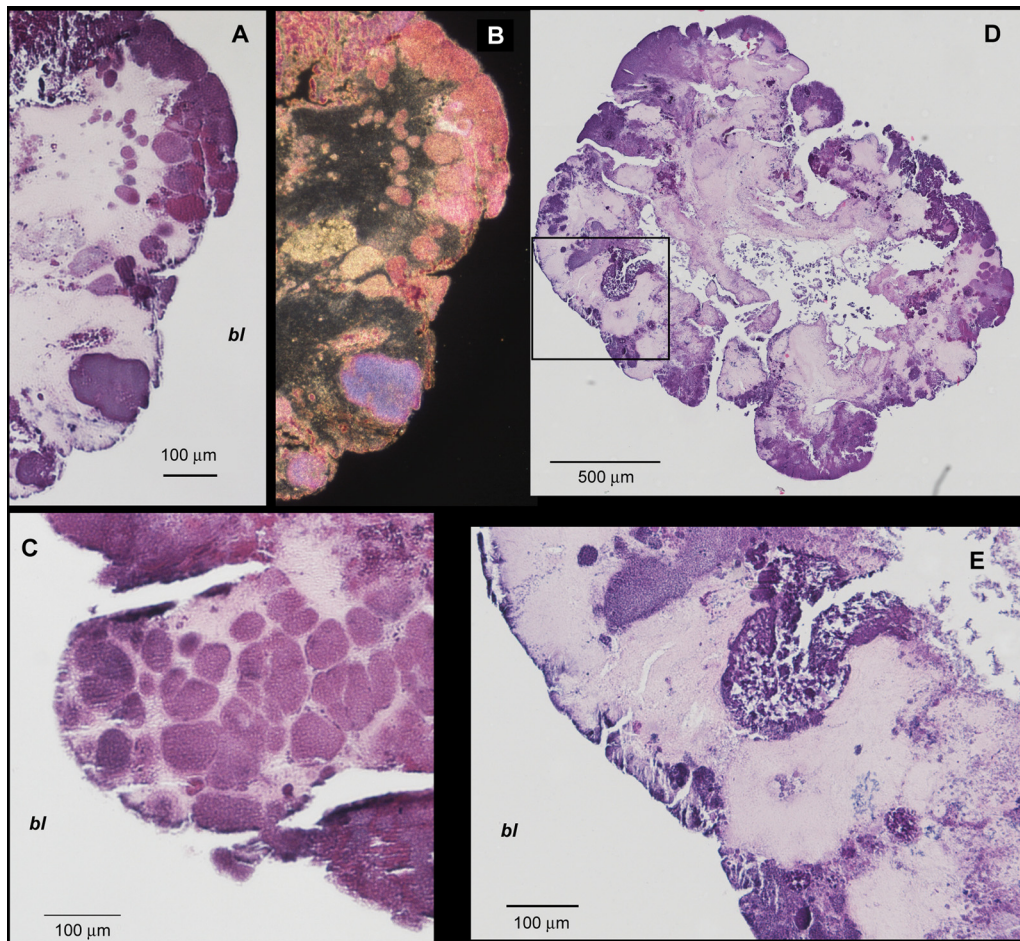
FIG 4 Bright-field microimages from thin sections obtained from the center of granules and stained with H&E. The "*bl*" refers to bulk liquid. (A to C) Images show that various types of dense microcolonies (dark pink/purple) are embedded in a matrix of less dense cellular material (light pink). (D) Overview of an entire granule showing a highly irrigated inner structure. (E) Zoom image corresponding to the inset square in panel D showing colonies irrigated by the inner channels.

Fluorescence images of cross-sectioned propionate-cultivated granules showed that the large cluster structures were mainly composed of *Accumulibacter*-type bacteria, which are known to accumulate polyphosphate and are commonly found in enhanced biological phosphorus removal systems. These structures often protuberated from the "periphery of the granule" (Fig. 2A). A contiguous section of identical granules examined by hematoxylin-eosin (H&E) staining and observed under bright (Fig. 2C) and dark (Fig. 2D) fields showed the spatial location of a clear glue-like exopolymeric material on the edge of parts of the granule. Similarly, fluorescence images of a large acetate-cultivated granule (3 to 4 mm in diameter) revealed that *Accumulibacter* also formed large cluster-structures which protuberated from the "periphery of the granule" (Fig. 3A and B). The H&E images (Fig. 3C and D) revealed the arrangement of cavities and the "root" of large clusters in the interior of the granules. In addition, these images showed that the overall structure of the granule was preserved after histological processing. In large granules, less substrate can penetrate, thus inherently less biomass can grow in the inner zones. The biomass present in those zones will eventually decay leaving empty spaces, thus the granule may become porous. Although further confirmation tests using imaging under more nat-

ural conditions (i.e., hydrated state) than what we used would be required, the granules in the present study show cavities, particularly in the inner zones (Fig. 3 and 4). The dense bacterial populations in the outer part of the granules are better contrasted in the dark-field mode in which they appear darker and closer in wavelength to the strong pink and purple color of the original H&E staining (Fig. 3C and D).

Images of a propionate-cultivated granule taken at the end of the experiment (day 380) revealed various types of colonies and heterogeneous cell densities even on the surface of the granule (Fig. 4A to C). Thin sections imaged from a complete granule sampled on day 380 showed visible signs of erosion, e.g., the surface of an "old" granule (Fig. 4D) appeared more irregular than that of "mature" granules sampled on day 169 (Fig. 2C and 3C). The "old" granules can most likely remain quasi-intact for long periods of time before splitting. The large cavities observed in the "old" granule allowed irrigation and growth of dense colonies along the paths of the channels (Fig. 4E). Hence, in some areas and along an *x* axis, paradoxically higher biomass was observed in the inner part of the granule compared to the outer part (Fig. 4E). Observations at higher magnification revealed in more detail the "root" of large clusters from the interior of the granules (Fig. 5).
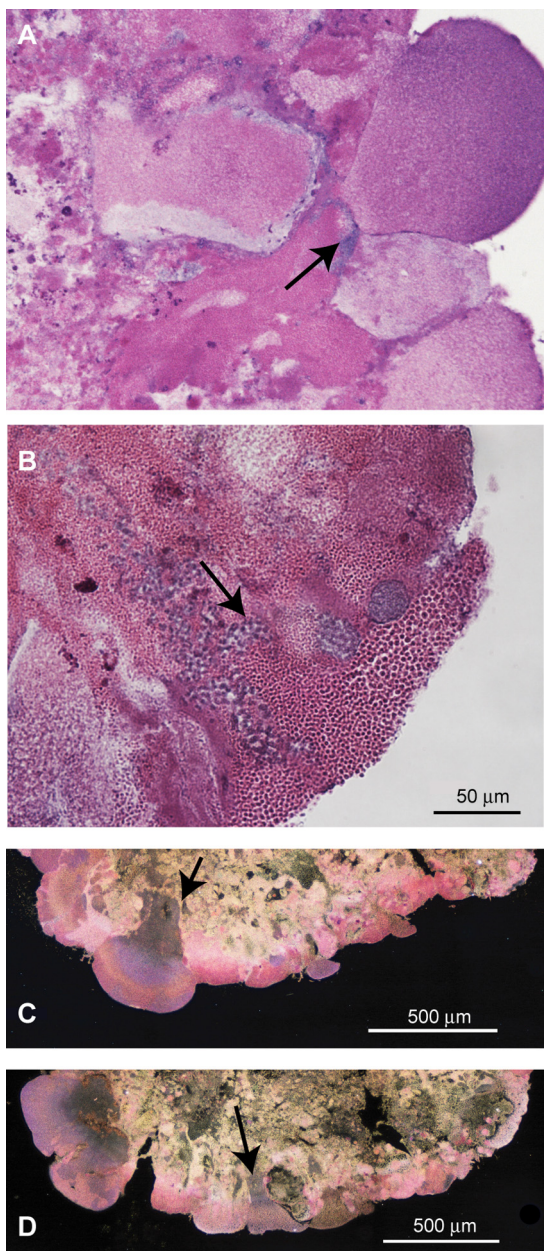
FIG 5 (A and B) Bright-field images, respectively, showing clusters of biomass that "root" or outgrow from the granule. The scale bar in panel B applies similarly to panel A. (C and D) Dark-field images showing similar shapes of outgrow of clusters observed in other granules. The arrows indicate the start of outgrows. The center of the granules is opposite to the arrows.
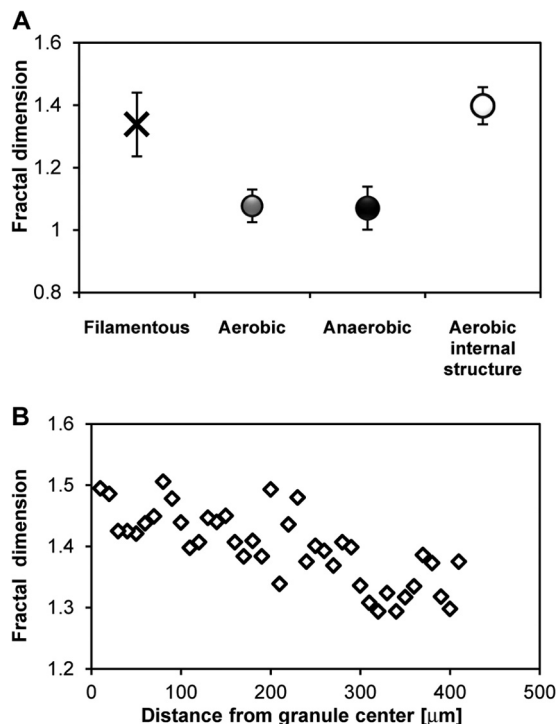

FIG 6 (A) Fractal dimension estimated for various types of granules. For comparisons, microscopic images of anaerobic granules previously reported (29) were used. (B) Fractal dimension as a function of distance from the granule center.

granules was 1.08 ± 0.05 (Fig. 6A). Stereomicroscopic images, however, do not display the internal structure-liquid interface of the granules. Hence, the fractal dimension (1.4 ± 0.06) was estimated from images acquired using thin sections obtained from the center of granules (Fig. 6A, aerobic internal structure) and tended to be higher (i.e., a more complex structure) than at the surface (Fig. 6B). The porosity as a function of the granule radial distance was estimated by using images from a series of thin slices. The space occupied by voids in the central zone of the granule was approximately 35 to 40%, whereas estimated porosities in the outer zone were as low as 10% (Fig. 7).

3D reconstruction. A 3D model based on the measured information may allow for a better understanding of substrate supply and intermediates transport within the cavern-like architecture of the granules (see Movie S1 in the supplemental material). Such models may offer the opportunity to explore the extent of dead-end pores and/or connectivity of the internal channeling structure. Because

FIG 7 Internal porosity as a function of distance from the center of the granule.

Surface and porosity characteristics of granules. Because of the importance of surface characteristics for the hydrodynamics at the solid-liquid interface (32) and the distinct surface characteristics observed in aerobic granules, we explored the possibility of quantifying the surface morphology at the granule structure-liquid interface reflected by the fractal dimension. Aerobic granules with an outer filamentous surface (i.e., hairy surface) are often observed in the initial phases during the granulation process. The estimated fractal dimension for this type of filamentous granules was 1.3 ± 0.1, whereas the fractal dimension of mature aerobic
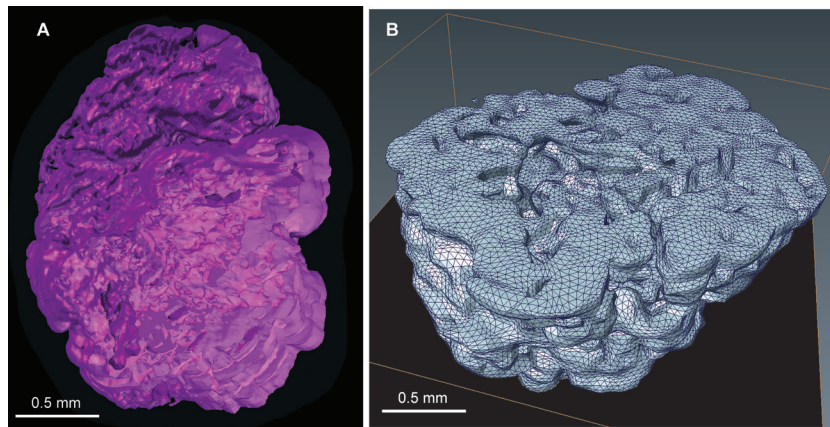
FIG 8 (A) 3D rendering of an aerobic granule. (B) Volumetric representation of half of a granule as tetrahedral grid. For this reconstruction, 41 slices of 12 μm each (see Fig. S2 in the supplemental material) were used.

these features are key determinants in fluid flow within the granule, a 3D model of the aerobic granule was obtained using a series of 2D images (see Fig. S2 in the supplemental material). The resulting 3D rendering allows a mesoscopic impression of the cavern-like interior structure of the granule (Fig. 8).

DISCUSSION

Theories for anaerobic (3) and aerobic granule (33) structure formation suggest that filamentous microorganisms serve as a backbone for granule structure. Also the floc-forming bacteria *Zoogloea* are key players in activated sludge flocs formation, and aerobic granules dominated by this genus have been cultivated (34, 35). Indeed, when the aerobic granules used in the present study were formed, our previous molecular analysis identified the presence of numerous filamentous bacteria (*Thiothrix* spp.) and floc-forming (e.g., *Zoogloea* spp.) bacteria (18). The young granular sludge was comprised of hairy-like granules and smooth granules (not shown) as previously reported for short-term studies on aerobic granules (33, 36). Eventually, most filamentous bacteria were outcompeted and washed out from the system, no longer determining granular structure. The few that were retained were found particularly in the less (shear) exposed surfaces of the mature granular structure (Fig. 1F). The mature aerobic granules (after 50 days) developed a cluster architecture. In our system, this cluster architecture did not seem to be the result of multiple microcolony aggregation as reported earlier (23) for aerobic granules because the clusters seem to "root" from the granule (Fig. 5). Notably, a cluster type structure with protuberated cell colonies was earlier documented for methanogenic granules treating brewery wastewater in full-scale reactors (29). Our distinct approach to observe contiguous sections of granules using different optical methods allowed detailed insights into the architecture of aerobic granules. These observations included that the clusters were mainly mono-colonies constituted by *Accumulibacter*. The H&E imaging (bright and dark fields) revealed that the clusters root (i.e., radial outgrows) from the granular structure. Protuberated large clusters might detach because they are more exposed to the fluid shear forces and particle collisions during aeration. These large clusters are still large (Fig. 2 and 3) and dense enough to be well retained within the system and serve as seed nuclei for the growth of a "new" granule. The *Accumulibacter* large clusters might be particularly dense because of the polyphosphate content compared to the *Competibacter* colonies. Since *Competibacter*-type bacteria are undesirable because they do not contribute to enhanced phosphorus removal, the large-cluster feature may give *Accumulibacter* a further distinct ecological advantage over *Competibacter* as small detached colonies of the latter might be prone to selective washout from the system.

Our results reveal that granules that have "lived" >300 days will show signs of erosion/detachment and clear inner biomass colonization because of substrate irrigation via highly developed channels (Fig. 4D and E). In the eventual breakage of the granule, the broken entity may contain a more diverse population compared to the detached cluster entity described above.

From the standpoint of engineering granules, one intriguing issue is how to couple the operational process previously known to select for certain process functions to the life cycle of granules. An interesting mathematical model proposed earlier (37) describes the growth of aerobic granules in a system similar to the one used in the present study. The simulation results for 334- and 700-day-old granules captured the general observations of higher biomass densities in the periphery of the granules. Although comparisons are difficult, the channel structure measured here and observed in the 3D reconstruction (which is not described by the existing model) and the high shearing forces of the system might suggest that most granules as single entities may not "live" 700 because ruptures and/or clusters detachments occur before this time. Also of note for modeling purposes is that the measured porosity is not constant, as often assumed, but a function of the granule's radius (Fig. 7). This is important because fluid flow is controlled by the distribution of porosity rather than by its average value. Although further tests are advisable to confirm our porosity estimates, a previous study using a thin section of the central zone of hydrated granules stained with cell- and extracellular polymeric substance (EPS)-specific stains showed that ca. 35% of the section area is cavities (38). The granules of that study were cultivated in a similar condition as our granular sludge sample for which we estimated a comparable porosity of ca. 35 to 40% at the center (Fig. 7). Our staining approach allows a high-quality contrast; hence, the limitations due to thresholding when estimating parameters, such as porosity, from image analysis are overcome. The tetrahedral grid generated from the granule measurements (images) can be con-

sidered a realistic geometry of the granule. Although it would be desirable/necessary to generate grids for a number of granules, such grids may be used as an input for modeling purposes.

Incorporating relevant phenomena of the life cycle of granular sludge, such as cluster detachment and associated new granule growth and channel formation with new growth zones, into existing models should be feasible. These phenomena particularly redefine the oxic-anoxic zones within granules which are important for simultaneous nitrogen and phosphorus removal. Although computationally demanding (37) and challenging from the standpoint of experimentally measuring all relevant parameters, these models should allow the virtual engineering of granules, which would without a doubt be a fascinating achievement.

ACKNOWLEDGMENT

REFERENCES

1. **Liu X-W, Sheng G-P, Yu H-Q.** 2009. Physicochemical characteristics of microbial granules. Biotechnol. Adv. **27:**1061–1070. http://dx.doi.org/10.1016/j.biotechadv.2009.05.020.
2. **Lettinga G, Vanvelsen AFM, Hobma SW, Dezeeuw W, Klapwijk A.** 1980. Use of the upflow sludge blanket (Usb) reactor concept for biological wastewater treatment, especially for anaerobic treatment. Biotechnol. Bioeng. **22:**699–734. http://dx.doi.org/10.1002/bit.260220402.
3. **Hulshoff-Pol LW, de Castro-Lopes SI, Lettinga G, Lens PNL.** 2004. Anaerobic sludge granulation. Water Res. **38:**1376–1389. http://dx.doi.org/10.1016/j.watres.2003.12.002.
4. **de Mes TZD, Stams AJM, Reith JH, Zeeman G.** 2003. Methane production by anaerobic digestion of wastewater and solid wastes, p 58–95. *In* Reith JH, Wijffels RH, Barten H (ed), Bio-methane and bio-hydrogen: status and perspectives of biological methane and hydrogen production. Smiet Offset, The Hague, Netherlands.
5. **de Kreuk MK, Kishida N, van Loosdrecht MCM.** 2007. Aerobic granular sludge: state of the art. Water Sci. Technol. **55**(8-9)**:**75–81.
6. **Adav SS, Lee D-J, Show K-Y, Tay J-H.** 2008. Aerobic granular sludge: recent advances. Biotechnol. Adv. **26:**411–423. http://dx.doi.org/10.1016/j.biotechadv.2008.05.002.
7. **de Kreuk M, Heijnen JJ, van Loosdrecht MCM.** 2005. Simultaneous COD, nitrogen, and phosphate removal by aerobic granular sludge. Biotechnol. Bioeng. **90:**761–769. http://dx.doi.org/10.1002/bit.20470.
8. **Ni B-J, Xie W-M, Liu S-G, Yu H-Q, Wang Y-Z, Wang G, Dai X-L.** 2009. Granulation of activated sludge in a pilot-scale sequencing batch reactor for the treatment of low-strength municipal wastewater. Water Res. **43:**751–761. http://dx.doi.org/10.1016/j.watres.2008.11.009.
9. **Xiao F, Yang SF, Li XY.** 2008. Physical and hydrodynamic properties of aerobic granules produced in sequencing batch reactors. Separation Purification Technol. **63:**634–641. http://dx.doi.org/10.1016/j.seppur.2008.07.002.
10. **de Bruin LMM, de Kreuk MK, van der Roest HFR, Uijterlinde C, van Loosdrecht MCM.** 2004. Aerobic granular sludge technology: an alternative to activated sludge? Water Sci. Technol. **49**(11-12)**:**1–7.
11. **Chen Y, Jiang W, Liang D, Tay J.** 2007. Structure and stability of aerobic granules cultivated under different shear force in sequencing batch reactors. Appl. Microbiol. Biotechnol. **76:**1199–1208. http://dx.doi.org/10.1007/s00253-007-1085-7.
12. **de Kreuk MK, Pronk M, van Loosdrecht MCM.** 2005. Formation of aerobic granules and conversion processes in an aerobic granular sludge reactor at moderate and low temperatures. Water Res. **39:**4476–4484. http://dx.doi.org/10.1016/j.watres.2005.08.031.
13. **Liu YQ, Tay JH.** 2007. Characteristics and stability of aerobic granules cultivated with different starvation time. Appl. Microbiol. Biotechnol. **75:**205–210. http://dx.doi.org/10.1007/s00253-006-0797-4.
14. **McSwain BS, Irvine RL, Wilderer PA.** 2004. The influence of of-settling time on the formation of aerobic granules. Water Sci. Technol. **50**(10)**:**195–202.
15. **Wang XH, Zhang HM, Yang FL, Xia LP, Gao MM.** 2007. Improved stability and performance of aerobic granules under stepwise increased selection pressure. Enzyme. Microb. Technol. **41:**205–211. http://dx.doi.org/10.1016/j.enzmictec.2007.01.005.
16. **Wang ZW, Li Y, Zhou JQ, Liu Y.** 2006. The influence of short-term starvation on aerobic granules. Process Biochem. **41:**2373–2378. http://dx.doi.org/10.1016/j.procbio.2006.06.009.
17. **Bassin JP, Pronk M, Kraan R, Kleerebezem R, van Loosdrecht MCM.** 2011. Ammonium adsorption in aerobic granular sludge, activated sludge and anammox granules. Water Res. **45:**5257–5265. http://dx.doi.org/10.1016/j.watres.2011.07.034.
18. **Gonzalez-Gil G, Holliger C.** 2011. Dynamics of microbial community structure of and enhanced biological phosphorus removal by aerobic granules cultivated on propionate or acetate. Appl. Environ. Microbiol. **77:**8041–8051. http://dx.doi.org/10.1128/AEM.05738-11.
19. **Li A-J, Yang S-F, Li X-Y, Gu J-D.** 2008. Microbial population dynamics during aerobic sludge granulation at different organic loading rates. Water Res. **42:**3552–3560. http://dx.doi.org/10.1016/j.watres.2008.05.005.
20. **de Kreuk MK, Picioreanu C, Hosseini M, Xavier JB, van Loosdrecht MCM.** 2007. Kinetic model of a granular sludge SBR: influences on nutrient removal. Biotechnol. Bioeng. **97:**801–815. http://dx.doi.org/10.1002/bit.21196.
21. **Su KZ, Yu HQ.** 2006. A generalized model for aerobic granule-based sequencing batch reactor. 2. Parametric sensitivity and model verification. Environ. Sci. Technol. **40:**4709–4713. http://dx.doi.org/10.1021/es060142e.
22. **Liu L, Sheng G-P, Liu Z-F, Li W-W, Zeng RJ, Lee D-J, Liu J-X, Yu H-Q.** 2010. Characterization of multiporous structure and oxygen transfer inside aerobic granules with the percolation model. Environ. Sci. Technol. **44:**8535–8540. http://dx.doi.org/10.1021/es102437a.
23. **Barr JJ, Cook AE, Bond PL.** 2010. Granule formation mechanisms within an aerobic wastewater system for phosphorus removal. Appl. Environ. Microbiol. **76:**7588–7597. http://dx.doi.org/10.1128/AEM.00864-10.
24. **Lemaire R, Webb RI, Yuan Z.** 2008. Micro-scale observations of the structure of aerobic microbial granules used for the treatment of nutrient-rich industrial wastewater. ISME J. **2:**528–541. http://dx.doi.org/10.1038/ismej.2008.12.
25. **Daims H, Stoecker K, Wagner M.** 2005. Fluorescence in situ hybridization for the detection of prokaryotes, p 213–239. *In* Osborn AM, Smith CJ (ed), Advanced methods in molecular microbial ecology. Bios-Garland, Abingdon, United Kingdom.
26. **Crocetti GR, Hugenholtz P, Bond PL, Schuler A, Keller J, Jenkins D, Blackall LL.** 2000. Identification of polyphosphate-accumulating organisms and design of 16S rRNA-directed probes for their detection and quantitation. Appl. Environ. Microbiol. **66:**1175–1182. http://dx.doi.org/10.1128/AEM.66.3.1175-1182.2000.
27. **Crocetti GR, Banfield JF, Keller J, Bond PL, Blackall LL.** 2002. Glycogen-accumulating organisms in laboratory-scale and full-scale wastewater treatment processes. Microbiology **148:**3353–3364.
28. **Kong YH, Ong SL, Ng WJ, Liu WT.** 2002. Diversity and distribution of a deeply branched novel proteobacterial group found in anaerobic-aerobic activated sludge processes. Environ. Microbiol. **4:**753–757. http://dx.doi.org/10.1046/j.1462-2920.2002.00357.x.
29. **Gonzalez-Gil G, Lens PNL, Van Aelst A, Van AH, Versprille AI, Lettinga G.** 2001. Cluster structure of anaerobic aggregates of an expanded granular sludge bed reactor. Appl. Environ. Microbiol. **67:**3683–3692. http://dx.doi.org/10.1128/AEM.67.8.3683-3692.2001.
30. **Rasband W.** 2005. ImageJ: image manipulation software. National Institutes of Health, Bethesda, MD. http://rsb.info.nih.gov/ij/.
31. **Doube M, Kłosowski MM, Arganda-Carreras I, Cordelieres FP, Dougherty RP, Jackson JS, Schmid B, Hutchinson JR, Shefelbine SJ.** 2010. BoneJ: free and extensible bone image analysis in ImageJ. Bone **47:**1076–1079. http://dx.doi.org/10.1016/j.bone.2010.08.023.
32. **Taherzadeh D, Picioreanu C, Küttler U, Simone A, Wall WA, Horn H.** 2010. Computational study of the drag and oscillatory movement of biofilm streamers in fast flows. Biotechnol. Bioeng. **105:**600–610. http://dx.doi.org/10.1002/bit.22551.
33. **Beun JJ, Hendriks A, Van Loosdrecht MCM, Morgenroth E, Wilderer PA, Heijnen JJ.** 1999. Aerobic granulation in a sequencing batch reactor. Water Res. **33:**2283–2290. http://dx.doi.org/10.1016/S0043-1354(98)00463-1.
34. **Wang X, Hu M, Xia Y, Wen X, Ding K.** 2012. Pyrosequencing analysis of bacterial diversity in 14 wastewater treatment systems in China. Appl. Environ. Microbiol. **78:**7042–7047. http://dx.doi.org/10.1128/AEM.01617-12.
35. **Weissbrodt DG, Neu TR, Kuhlicke U, Rappaz Y, Holliger C.** 2013. Assessment of bacterial and structural dynamics in aerobic granular biofilms. Front. Microbiol. **4:**1–18.

36. **Beun JJ, van Loosdrecht MCM, Heijnen JJ.** 2002. Aerobic granulation in a sequencing batch airlift reactor. Water Res. **36:**702–712. http://dx.doi .org/10.1016/S0043-1354(01)00250-0.

37. **Xavier JB, de Kreuk MK, Picioreanu C, van Loosdrecht MCM.** 2007. Multiscale individual-based model of microbial and bioconversion dynamics in aerobic granular sludge. Environ. Sci. Technol. **41:**6410–6417. http://dx.doi.org/10.1021/es070264m.

38. **Chen MY, Lee DJ, Tay JH.** 2007. Distribution of extracellular polymeric substances in aerobic granules. Appl. Microbiol. Biotechnol. **73:**1463–1469. http://dx.doi.org/10.1007/s00253-006-0617-x.

39. **King R, George A, Jeon T, Hynan L, Youn T, Kennedy D, Dickerson B.** 2009. Characterization of atrophic changes in the cerebral cortex using fractal dimensional analysis. Brain Imag. Behav. **3:**154–166. http://dx.doi .org/10.1007/s11682-008-9057-9.